ELSEVIER

Astroparticle Physics 8 (1997) 27–42

Astroparticle Physics

OMNIS—an improved low-cost detector to measure mass and mixing of mu/tau neutrinos from a Galactic supernova

P.F. Smith

Rutherford Appleton Laboratory, Chilton, Oxfordshire, OX11 0QX, UK

Received 29 January 1997; revised 20 August 1997

Abstract

OMNIS is an observatory for multiflavour interactions from Galactic supernovae. It has evolved from the Supernova Neutrino Burst Observatory (SNBO) proposed by Cline et al., based on the detection of the neutrinos by neutral current nuclear excitation in natural rock. This would result in the emission of neutrons, which could be captured by counters embedded in the rock. This scheme would be sensitive principally to the higher temperature μ and τ neutrinos and would allow time-of-flight measurement of neutrino mass if in the cosmologically interesting range 10–100 eV. The present paper proposes a new neutron detection arrangement which improves detection efficiency and reduces cost by a factor ~ 30, allowing the time profile of over 2000 $\nu_{\mu\tau}$ events to be recorded with only 200 tons scintillator. This new scheme represents the optimum configuration for a natural underground rock target. A Galactic supernova signal would be a factor 10–30 above neutron background (from cosmic ray muons and alpha activity) in sites with depth > 500 mwe. Another major improvement results by supplementing the rock with more favourable target elements such as iron or lead, giving sensitivity to all three neutrino types and mixing between these. Some calculations are included on the speculative possibility of extra-Galactic supernova neutrino detection using this principle. © 1997 Elsevier Science B.V.

Keywords: Galactic supernova; SNBO (Supernova Neutrino Burst Observatory); Neutrino

1. Supernova neutrinos

A type II (or Ib) supernova explosion releases most of its energy as neutrinos and antineutrinos with a time constant of a few seconds [1–6]. All three neutrino types and their antiparticles are produced in comparable numbers. Of a total of typically $3 \cdot 10^{53}$ ergs released, about 40% is released as $\nu_e + \bar{\nu}_e$, 30% as $\nu_\mu + \bar{\nu}_\mu$ and 30% as $\nu_\tau + \bar{\nu}_\tau$ [3]. The explosion mechanisms and the resulting time and energy profile of the emitted neutrinos, are also known with reasonable accuracy. This provides a unique opportunity to discover neutrino properties which are difficult or impossible to determine using terrestrial neutrino sources. In particular, a non-zero neutrino mass will alter the time profile arriving at the earth, offering the possibility of direct time-of-flight measurement of the mass of at least one neutrino type.

Moreover, the most likely distance range for Galactic supernovae ($\sim$ 2–20 kpc) happens to be ideal for time-of-flight measurement of a 'cosmologically significant' neutrino mass—i.e., a mass in the range 10–100 eV. Such a mass range is of major interest to both particle physics and astronomy for two reasons.

PII S0927-6505(97)00041-8

(i) For the average neutrino density $\approx 100\ (\nu + \bar{\nu})/\mathrm{cm}^3$/generation, predicted from decoupling in the early universe at time ~ 1 s ($T \approx 1$ MeV), the contribution Ω_ν of neutrinos to the total density parameter Ω is related to the neutrino masses by [7]

$$m(\nu_\tau) + m(\nu_\mu) + m(\nu_e) \approx 100(h_{100})^2 \Omega_\nu \qquad (1)$$

where h_{100} = Hubble constant/100 km s^{-1} Mpc^{-1}.

Thus if one mass dominates, a value 25–100 eV could close the universe.

(ii) A neutrino mass $\approx$ 25–30 eV, if clustered in the Galaxy, could account for the dark matter component, at the same time being consistent with the required Galactic velocity and the phase space density at decoupling [8,9].

Fig. 1 shows the locations of known supernovae in our Galaxy during the past 1000 yr [6], as a reminder that only those within a few kpc of the sun are visible optically. In contrast, a neutrino observatory would detect the much larger number occurring in the whole Galaxy. The 4–5 II or Ib supernovae recorded in 1000 y within 4 kpc of the sun (5% of the Galaxy) is consistent with a total supernova frequency in the Galaxy as high as ≈ 0.06–0.1 yr^{-1} [6,10,11]. Thus, on the basis of the observed numbers the next Galactic supernova is likely to occur within 10–20 yr, which is not dissimilar to the timescale of many terrestrial particle physics and particle astrophysics projects.

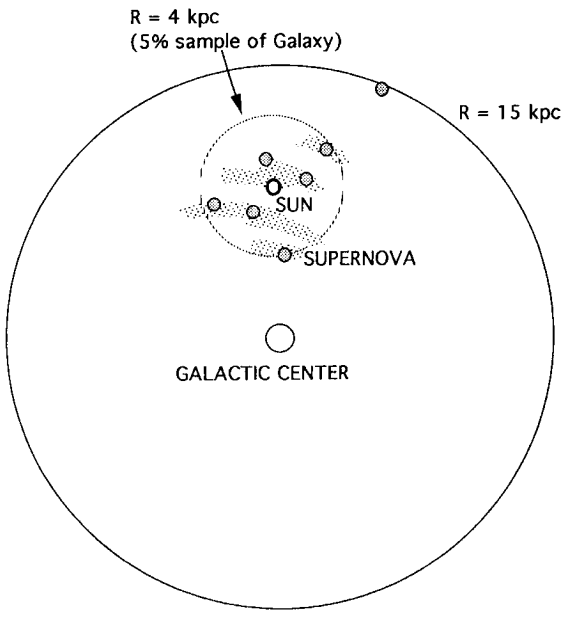

Fig. 1. Plan view of Galaxy showing locations of visible supernovae in the past 1000 yr (from Ref. [6]).

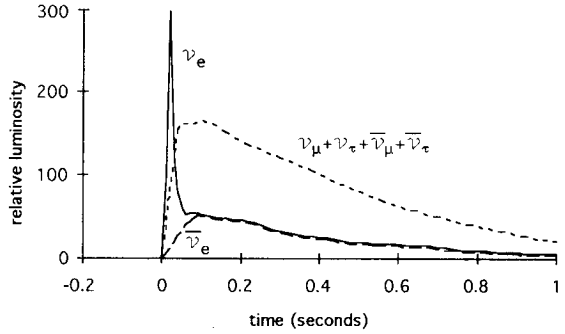

Fig. 2. Relative luminosity (arbitrary units) vs. time for each neutrino type (from Ref. [14]).

Fig. 2 shows a typical computed time profile for the emission of each neutrino type [14]. The momentum spectrum is approximately Fermi–Dirac with mean temperatures ≈ 11 MeV for ν_e, ≈ 16 MeV for $\bar{\nu}_e$ and ≈ 25 MeV for $\nu_\mu \bar{\nu}_\mu \nu_\tau \bar{\nu}_\tau$ [14]. These temperatures vary slightly with the theoretical model, but the expectation that the mu/tau neutrino temperature is substantially higher than the electron neutrino temperature is a basic consequence of the neutrino production processes and is common to all models. Also common to all models is the expectation that (in the absence of mixing) ν_μ and ν_τ are produced with nearly identical time profiles and momentum spectra. Neutrino mass measurement is then based on the fact that a difference between ν_μ and ν_τ masses will result in different velocities for a given momentum, causing their time profiles to both spread and separate due to the difference in travel times. For illustrative purposes we assume the mass hierarchy $m(\nu_\tau) \gg m(\nu_\mu) \gg m(\nu_e)$. The time delay for a ν_τ of mass $m(\nu_\tau)$ and energy $E(\nu_\tau)$ is then

$$\Delta t(s) \approx 0.05[R/1\,\mathrm{kpc}][m(\nu_\tau)/1\,\mathrm{eV}]^2 \times [1\,\mathrm{MeV}/E(\nu_\tau)]^2 \qquad (2)$$

Integrating over the whole spectrum, the appearance of the combined $(\nu_\mu + \nu_\tau)$ arrival time profile is illustrated in Fig. 3 for the cases $m(\nu_\tau) = 50$ eV, $m(\nu_\tau) = 25$ eV and $m(\nu_\tau) = \ll 10$ eV, for a distance $R = 8$ kpc (the characteristic distance for a Galactic

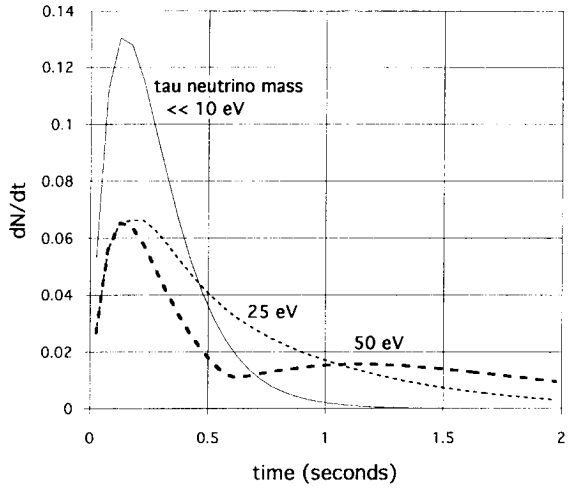

Fig. 3. Arrival time profile for mu and tau neutrinos from supernova at 8 kpc, showing effect of non-zero tau neutrino mass.

supernova, similar to the distance to the Galactic centre). The ν_μ and ν_τ profiles become distinct for a mass difference > 20 eV and with a sufficient number of events (≥ 2000) can also be separated analytically at lower masses, at least down to 5 eV.

Other neutrino physics can also be deduced from the supernova signal. Since the emitted proportions of the three neutrino types are approximately known, observation of all three time profiles and event numbers would provide unique information on any mixing between the three types, either through vacuum oscillations over the travel distance or matter oscillations within the supernova itself [12,13].

Because of Poisson fluctuations in the event time distribution (see example in Section 7 below) the extraction of estimates of neutrino masses and mixing from a supernova signal with a high confidence level requires ~ 1000 events of each of the three neutrino flavours. A number of existing world detectors are sensitive to supernova neutrinos, in particular Super-Kamiokande, LVD, MACRO and SNO. However, these detect principally the $\bar{\nu}_e$ component through charged current interactions and have relatively low sensitivity to neutral current events [3]. Numerical estimates are summarised in Section 8 (Table 1) showing that from an 8 kpc supernova Super-Kamiokande would provide ~ 8000 $\bar{\nu}_e$ events, but only 1% of that number from $\nu_{\mu\tau}$. The purpose of this paper is to discuss the evolution of a low cost detection scheme which would be sensitive principally to the $\nu_{\mu\tau}$ component of a supernova signal. This would provide the first direct observation and measurement of a cosmologically significant ν_τ or ν_μ mass and would complement the ν_e, $\bar{\nu}_e$ signal from other world detectors to provide data on mixing effects between all three neutrino generations.

2. The SNBO concept

It was first proposed by Cline et al. [12,13] that natural rock could be used as a target for supernova

Table 1
Comparison of proposed OMNIS multi-target observatory with world detectors based on direct detection with water and scintillator targets. Approximate event numbers for each neutrino type shown for a supernova at 8 kpc

	Target material	Fiducial mass (ton)	Target elements	ν_e	$\bar{\nu}_e$	$\nu_{\mu,\tau} + \bar{\nu}_{\mu,\tau}$
Combined target / detector:						
Super-Kamiokande	H_2O	32000	p,e,O	180	8300	50
LVD	CH_2	1200	p,e,C	14	540	30
MACRO	CH_2	1000	p,e,C	8	350	25
SNO	H_2O	1600	p,e,O	16	520	6
SNO	D_2O	1000[a]	d,e,O	190	180	300[a]
Separated target and detector:						
OMNIS 200 t scintillator +	NaCl (rock)	8000	Na,Cl	10	10	400
Natural rock +	Fe	4000	Fe	10	10	600
Installed targets	Pb	4000	Pb	280	30	1000
			totals	**300**	**50**	**2000**
Direct interaction with scintillator	CH_2	200	p,e,C	2	70	5

[a] D_2O target not available indefinitely.

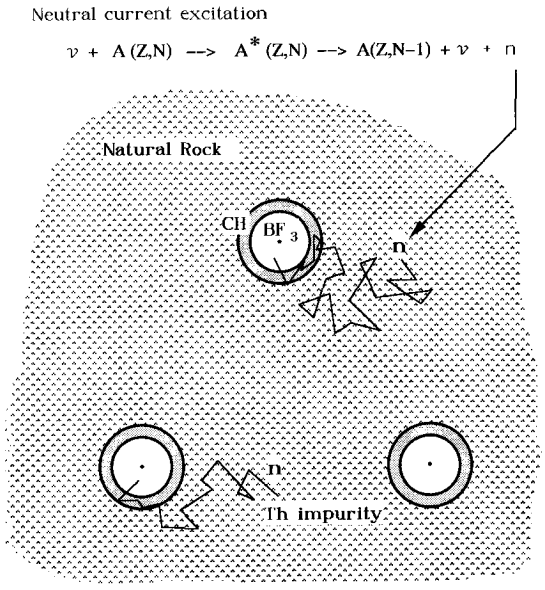

Fig. 4. Original SNBO concept, based on detection of emitted neutrons with boron trifluoride counters embedded in natural rock target. Typical neutron background event also shown, arising from α interaction.

neutrinos, using neutral current inelastic scattering to produce an excited nuclear state which decays with release of one or more neutrons. Neutron detectors embedded in the rock (Fig. 4) would thermalise and capture a substantial fraction of these (typically 20% of those produced within 0.5 m of the detector) in a time < 1 ms, so that the neutron time profile would represent also the time profile for neutrinos arriving at the Earth. In addition to the use of any natural underground material (e.g., chalk, salt, sandstone) as target, a key feature of this idea is that the energy dependence of the excitation cross section ($\alpha\ (E - E_0)^2$ where E_0 is a threshold energy) gives a signal resulting mainly from the higher energy mu/tau neutrinos, making this the only detection principle sensitive principally to the $\nu_{\mu\tau}$ component [14].

The generic name for this scheme, 'Supernova Neutrino Burst Observatory' (SNBO) reflected its aim to be a permanent supernova observatory, in contrast to detectors with a limited planned lifetime such as SNO, for which supernova detection is subsidiary to the main objective of solar neutrino observation.

For numerical studies of this scheme, a basic requirement is the neutron production per unit mass of target material, obtained by combining the predicted neutrino flux with the calculated nuclear excitation cross section and branching ratio for decay to neutrons [15–17,14]. Results presented in [14] contain some misprints [1] but a recent recalculation [27,18] gives, for a supernova at 8 kpc, a total production $6 \cdot 10^{-8}$ neutrons/g in NaCl, using an average branching ratio to neutrons of 10% [18]. This is typical also of other underground rock constituents such as $CaCO_3$ or SiO_2. Further calculations in progress suggest that multiple neutron emission may increase this by up to a factor 2, so that a nominal production $1 \cdot 10^{-7}$/g can be assumed for the average Galactic supernova, approximately independent of target material. [2]

This enables estimates to be made of the amount of detecting material needed to observe a given number of neutrino events. The neutron energy spectrum from de-excitation of the nucleus is assumed to be of the form:

$$\mathrm{d}N/\mathrm{d}E = (N_0/E_0)(2/\pi)^{0.5}(E/E_0)^{0.5} \times \exp(-E/E_0) \qquad (3)$$

where N_0 is the total production $1 \cdot 10^{-7}$/g and the characteristic energy E_0 is 1–2 MeV. Neither the value of E_0 or the precise form of Eq. (3) is critical for subsequent calculations, since the neutrons are moderated to near-thermal energies prior to detection.

For the present work, new Monte Carlo simulations have been carried out for the original suggestion [12,13] of standard 20 cm diameter BF_3 neutron proportional counters (enclosed by a few cm of thermalising hydrocarbon) distributed throughout the rock target. These show that an average of one neutron would be detected per 90 m length of detector, thus requiring 90 km rock-embedded detector for 1000 events, at a likely cost $> 3 \cdot 10^3$ £/m. Thus the SNBO scheme in its generic form turns out to be much more costly than originally anticipated, despite it's conceptual simplicity and zero-cost target material. However, by studies of alternative detector materials and optimised collection geometries it will be

[1] In particular, Fig. 3 of Ref. [14] should not be used [28].

[2] Heavy elements can give higher neutron production, see below.

shown in Section 3 that it is possible to achieve a series of improvements totalling a factor ~ 30 gain in efficiency and cost.

3. Optimisation of neutron detection

Studies of neutron transport, thermalisation and detection are carried out with a Monte Carlo programme able to simulate one or more detectors in an underground cavern, or in the rock itself. The detector and rock may consist of any combination of elements. For each element the programme contains a close approximation to the energy-dependence of neutron scattering and absorption cross sections. Neutrons are randomly chosen from the energy distribution of Eq. (3). Each is tracked from a random point of origin in the rock, given a random centre-of-mass scattering angle at each collision, progressively losing energy until absorbed (usually at or near thermal energy) in either the detector or the rock. Above 1 MeV, approximations to inelastic and non-isotropic scattering are also included, although this affects only the first few scatterings out of the several hundred needed to thermalise the neutrons before capture. An on-line display of the neutron tracks assists in understanding the detection process and its optimisation.

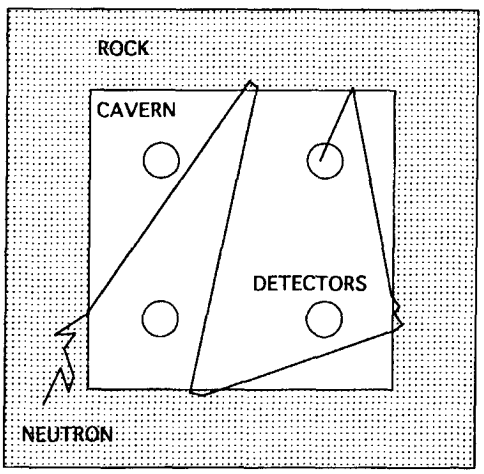

Fig. 5. Detection enhancement by multiple scattering in open cavern. Typical neutron path from emission in rock wall to thermalisation and capture in detector.

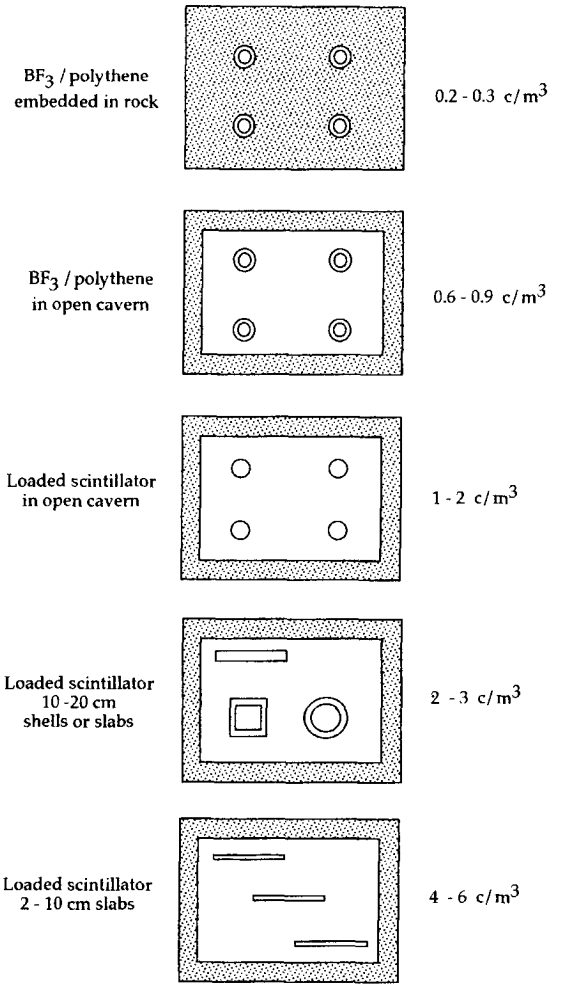

Fig. 6. Sequence of simulated detector arrangements. Typical improvements at each stage are shown as counts/m^3 detector for an 8 kpc supernova with neutron production 0.1/ton in salt rock (shaded areas).

This program was used first to simulate the proposed rock-embedded BF_3 counters of the SNBO proposal, giving the result already discussed in Section 2. To compare the efficiency of detection systems, it is convenient to express results as neutrons captured per cubic metre of detector for an 8 kpc supernova. Results for cylindrical BF_3 counters in NaCl rock are in the range 0.25 ± 0.05 neutrons/m^3 (dependent somewhat on detector diameter) for our nominal estimate of 10^{-7} neutrons per gram of rock. The objective is to devise detection systems which

will substantially increase this number. Improvements can be achieved in three distinct ways.

(1) If the detectors, instead of being embedded in the target material, are placed in a large open cavern, a gain results from multiple scattering around the cavern, giving several opportunities for detection before being absorbed in the rock (Fig. 5). For simulations, a cavern 10 m × 8 m × 6 m was used, typical of a salt mine. These multiple traversals give the appearance of diffuse reflection from the walls, but it is not true reflection-a neutron entering the wall simply makes a random walk which can result in re-emergence into the open cavern giving a straight-line path to another wall. This continues until the neutron is thermalised and absorbed in either detector or wall material. The number of such 'reflections' of an individual neutron can exceed 20 in some cases, but for the majority, it is in the range 2–5 'reflections' for NaCl walls. This effectively increases the flux of neutrons in the cavern and Monte Carlo studies confirm an increase in the number detected, by a factor 3. The dependence of this factor on the wall material is discussed in Section 5.

(2) The majority of neutrons emerging from the rock into the cavern still have energies in the keV to MeV range and need to be moderated to near-thermal energy for detection. In a BF_3 gas counter, thermalisation is provided by a surrounding wax or polythene cylinder, but a substantial proportion of the thermalised neutrons are then absorbed by the hydrogen before reaching the counter gas. More efficient detection is thus expected from a hydrocarbon scintillator (liquid or plastic) which acts both as moderator and detector. Neutrons will be absorbed by the hydrogen to produce a single 2.2 MeV gamma which, however, may not be easily separated from background gammas of similar energy coming from U and Th in the rock. For unambiguous neutron detection an organic scintillator can be loaded with Gd, ^{6}Li, or ^{10}B which have high neutron absorption cross sections and provide a higher energy distinctive scintillation signal [19–21,29]. For example, using liquid scintillator containing ≈ 0.2% Gd increases the neutron count in 20–30 cm diameter cylindrical detectors by a further factor 3 compared with BF_3 proportional counters. Note that increasing the loading beyond 0.2% does not significantly increase the number of neutrons captured, but increases the fraction absorbed on Gd rather than on H. For (0.1%, 0.2%, 0.5%) Gd, approximately (86%, 92%, 97%) of neutrons are captured by the Gd. Similar considerations apply to loading with Li and B.

(3) Cylindrical (or square) section detectors,

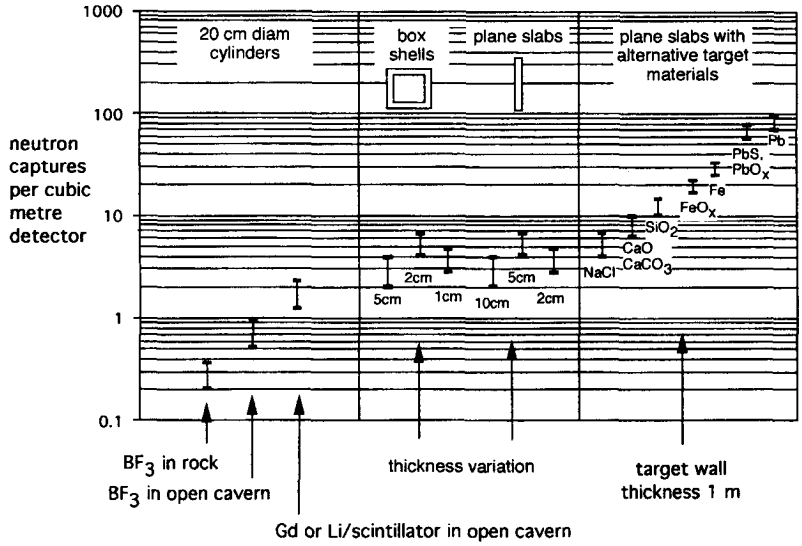

Fig. 7. Summary of improvements in neutron detection from an NaCl rock target through use of loaded scintillator, open geometry, and optimum surface/thickness, and using alternative target elements lining the cavern. For comparison purposes, a fixed production of 0.1 neutrons/ton is used for each target.

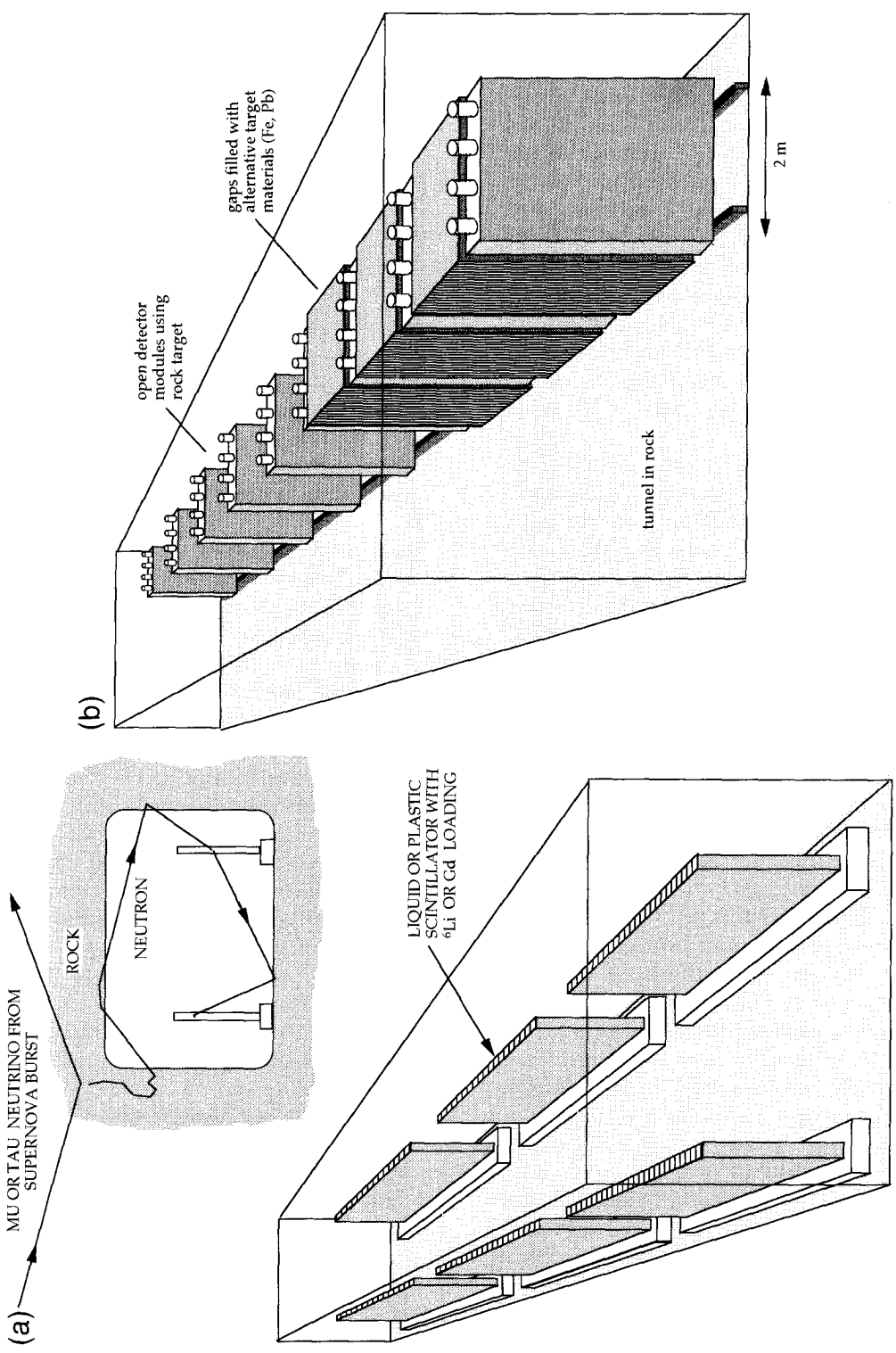

Fig. 8. (a) Illustrative detector arrangement for rock target, showing scintillator modules distributed along rock tunnel. (b) Possible detector arrangement for OMNIS multitarget system, showing scintillator modules alternating with target slabs, or left open for rock target.

though practically the most convenient, are the least effective geometry for neutron thermalisation and capture for a given volume of detector. This is partly because they have minimum surface area/volume and partly because they do not take sufficient advantage of the multiple traversals of neutrons in the cavern. Increasing the surface area exposed to the cavern walls and reducing detector thickness, improves the thermalisation and capture for a given detector volume. Two practical geometries have been investigated: (a) an annular space between two concentric cylinders or boxes, with optimisation of the diameter and thickness of detector material and (b) single plane slabs of varying thickness. Case (a) is also equivalent to several plane slabs in the same location.

Fig. 6 illustrates the series of geometries investigated and the typical improvements in count rate. Fig. 7 summarises the numerical results in more detail. The left hand portion of the chart shows the gains achieved in stages (1) and (2) above and the centre portion of the chart shows the effect of varying detector thickness in the 'annular box' or 'plane slab' configurations. The right hand portion of Fig. 7 shows the effect of alternative target materials and is discussed in Section 5 below.

We can conclude that the optimum detection geometry for the rock target would consist of large area and relatively thin slabs (5–10 cm thickness) of loaded scintillator distributed along open caverns (Fig. 8a). This arrangement achieves a factor 20 increase in neutron collection (≈ 6 events/m^3) compared with the original SNBO (≈ 0.3 events/m^3). It is important to note that for maximum collection efficiency the slabs should be distributed along the tunnel rather than located in the same region, where they share the same neutron flux and compete for the same events. In addition, because the neutrons are scattering between the walls and may pass through the detector more than once while degrading to thermal energy, two slabs in the same region are approximately equivalent to one thicker slab and there is then some departure from optimum. This can also be seen from comparison of single slabs with boxes ($\equiv$ 4–6 slabs) in Fig. 7, showing that the latter have a slightly lower optimum although the difference is not great. The ideal would be to allow each detecting slab to 'see' as much unobstructed cavern wall as possible, but space limitations may necessitate some practical compromises. This will require additional Monte Carlo studies for any specific location and rock material.

4. Choice of neutron absorber

The preceding calculations were carried out for a hydrocarbon scintillator (liquid or plastic) loaded with Gd, but apply equally to loading with ^{6}Li or ^{10}B. Adding sufficient (0.1%–1%) Gd, ^{6}Li, or ^{10}B to dominate the neutron capture usefully increases the total absorption cross section of the material but its principal purpose is to provide a clear signal to identify the neutron absorption event. ^{6}Li absorbs a neutron to produce a triton (energy 2.7 MeV, range 35 μm) and an α-particle (energy 2.1 MeV, range 5 μm).

Most of these events are contained within the scintillator to give a 4.8 MeV single line, but which is 'quenched' to 530 keV [20]. Similarly ^{10}B events yield a contained alpha +Li nucleus totalling 2.8 MeV, again quenched to lower energy [21,29]. Gd emits several gammas totalling about 8 MeV, well above the energy of background gammas from radioactivity [19], but with a Compton attenuation length in liquid scintillator $\approx$ 15–25 cm, so for the 'optimum' thickness of detector material indicated by Fig. 7 ($<$ 5 cm) only some variable fraction of the gamma energy will be detected and there may not be clear identification of the neutron events. This difficulty also applies to a non-loaded scintillator, which captures neutrons on hydrogen with the release of a 2.2 MeV gamma. From these simple arguments it appears that the localised event containment of the ^{6}Li or ^{10}B reactions is better matched to the optimum capture geometry, but that better neutron identification may be possible by using Gd loading and greater thicknesses of scintillator.

It should be emphasised that 'optimum geometry' has been studied here solely in terms of the events per unit volume of detector material, whereas in practice the cost of mechanical support, photomultiplier or solid state light detection and associated electronics, may increase with detector area and could shift the cost optimum towards fewer units with increased scintillator thickness.

5. Use of alternative or additional target materials—OMNIS

The neutral current excitation of nuclei by the supernova neutrinos has a cross section per nucleon which is approximately independent of the target nucleus [16,17]. Thus the neutron production per unit target mass should be dependent on target material mainly through variations in the branching ratio to neutrons [15] and the basic figure $\approx 1.10^{-7}$/g estimated for NaCl will be assumed to apply approximately to other natural rock materials ($CaCO_3$, SiO_2) but will be larger by a factor ~ 2 for Fe and by a factor ~ 4–6 for Pb [16,17,22,23].

Nevertheless the number of neutrons actually captured by a given detector geometry is quite strongly dependent on the target material. This is because after each neutron is produced there are two competing processes for its recapture: absorption in the cavern wall and absorption in the detector material. Thus if materials of lower neutron absorption cross section can be used, this will increase the fraction captured in the detector. Alternative or additional materials can be result in three ways:

1. use of different underground locations,
2. lining the cavern walls (effectively replacing the rock if > 50 cm thick),
3. placing selected materials in the cavern or around the detector.

A series of Monte Carlo simulations was carried out for a 1 m thickness of each alternative material, covering all walls of a 10 m × 8 m × 6 m cavern. The resulting events/m^3 detector are shown in the right hand segment of Fig. 7. This shows that the various natural rocks are rather similar from a neutron collection viewpoint. NaCl rock is one of the poorest because of the high neutron capture cross section of Cl, but nevertheless has the merit of the lowest neutron and gamma background (see below). Gains of up to a factor 2 in neutron collection may be achievable with rocks based on SiO_2 or CaO. A factor ~ 3–4 gain in collection efficiency would result from the use of Fe or Fe ores, with up to a factor ~ 10 gain from Pb or Pb ores. The latter also give higher neutron production and sensitivity to ν_e through charged current excitation [16,17,22,23]. The most effective scheme would utilise several target materials, e.g., Pb, Fe and rock, to distinguish neutrino flavour mixing effects. This multi-target version is thus an observatory for multiflavour interactions from supernovae (OMNIS). A possible detector/target configuration is illustrated in Fig. 8b.

Note that gains of up to a factor 2–3 could be achieved simply by stacking iron or lead (or their compounds) even in scrap form, somewhere in the cavern. This is because the neutrons traverse the cavern several times and any materials which rescatter them with reduced absorption probability will increase the chance of capture by the detector. However, layers smaller than ~ 50 cm will be less effective, since the full gain from multiple scattering in the cavern requires a thickness exceeding the random walk distance in the material, as discussed below. Thinner layers are more 'transparent' to neutrons and the underlying cavern material then dominates the scattering and wall absorption.

From the Monte Carlo simulations it is apparent that the improvements from the use of supplementary materials are approximately proportional to the survival distance or effective range l_s (g cm^{-2}) of neutrons before recapture, which thus represents a 'figure of merit' by which different target materials can be compared. It is possible to derive an approximate formula which relates l_s to the scattering and absorption cross sections of the constituent elements.

For a material of density ρ g cm^{-3} containing elements A_n in atomic proportions f_n, with mean elastic scattering [3] cross section σ_{sn} (barns), the scattering length l_s (in g cm^{-2}) is given by

$$1/l_s = 0.6\rho \sum_n f_n \sigma_{sn} / \sum_n f_n A_n \qquad (4)$$

Similarly the absorption length is approximately

$$1/l_a = 0.6\rho \sum_n f_n \sigma_{an} / \sum_n f_n A_n \qquad (5)$$

At each collision the mean fractional energy loss (given by centre of mass scattering angle 90°) is

[3] Inelastic scattering also contributes above 1 MeV, but the six decades of energy loss needed to reach the thermal region < 1 eV will be dominated by elastic scattering.

Table 2
Comparison of survival distances (projected range) of neutrons in various materials, from an initial energy of 1–10 MeV to capture in the same material. Thermalisation and capture lengths estimated from Eqs. (4), (5), (6a), (6b), (7) and (8)

Material	Density ($g\ cm^{-3}$)	Average number of scatters	Average scattering length ($g\ cm^{-2}$)	Projected range ($g\ cm^{-2}$)	Projected range (cm)
Metallic targets					
Pb	11.3	1800	34.5	860	76
PbO	9.0	500	26.5	350	39
Fe	7.9	500	13.3	170	22
FeO	5.0	280	10.9	110	22
Rock targets					
CaO	3.3	250	11.7	110	33
SiO_2	2.6	230	9.5	90	35
$CaCO_3$	2.9	230	8.1	80	28
NaCl	2.2	200	9.7	80	36
Other targets					
H_2O	1	140	0.83	5.6	5.6
Solid CO_2	1.5	3000	5.8	185	123
Scintillators					
CH_2	1	134	0.64	4.3	4.3
$CH_2 + 0.1\%\ ^6Li$	1	90	0.64	3.5	3.5
$CH_2 + 0.2\%\ ^6Li$	1	85	0.64	3.4	3.4
$CH_2 + 0.5\%\ ^6Li$	1	81	0.64	3.3	3.3
$CH_2 + 1.0\%\ ^6Li$	1	80	0.64	3.3	3.3

$\Delta_n = 2A_n/(1+A_n)^2$ so that the fraction of the initial energy E_0 remaining after N_s scatterings is

$$E/E_0 \approx \prod_n [1-\Delta] w_n N_s$$

$$\text{with } w_n = f_n \sigma_{sn} / \sum_n f_n \sigma_{sn} \qquad (6a)$$

which can be rewritten

$$\log(E/E_0) \approx N_s \sum_n w_n \log[(1-\Delta_n)] \qquad (6b)$$

As the energy decreases, the scattering cross section stays approximately constant (in order of magnitude) while the absorption cross section rises, typically as $E^{-0.5}$ until the thermal absorption cross section $\sigma_a(E_{th})$ is reached at the equilibrium thermal energy E_{th}:

$$\sigma_a(E) \approx \sigma_a(E_{th})[E_{th}/E]^{0.5} \qquad (7)$$

Thus the energy loss continues to a value E_a either at which $l_a(E_a) \approx l_s$, or at which $E_a = E_{th}$ ($= 0.023$ eV), whichever is the higher energy. Substituting $E = E_a$ in Eq. (6b) then gives an estimate of $N_s(E_a)$, the total number of scatters required to degrade the neutron energy from E_0 to E_a, after which absorption of the neutron requires on average a further $N_s(\text{cap}) \approx l_a/l_s$ scatters, giving a total number of scatters $N_s(\text{tot}) \approx N_s(E_a) + N_s(\text{cap})$ from production to capture.

Since this is a random walk, the neutron range will be of order

$$L_s(g\,cm^{-2}) \approx [N_s(\text{tot})]^{0.5} l_s \qquad (8)$$

The projected range perpendicular to the cavern wall (an indication of the thickness of material required) will be approximately $(1/\sqrt{3})L_s$ ($g\ cm^{-2}$) corresponding to a distance $(1/\sqrt{3})L_s/\rho$ (cm).

Table 2 summarises the results of this procedure for several target and detector materials, including those in Fig. 7. The collision numbers and ranges are expected to be rough estimates only, in particular where there are several elements with different energy dependence of the scattering cross section. Nevertheless the ranking of the materials in terms of neutron survival distance in $g\ cm^{-1}$ does correspond closely to the ranking in Fig. 7 from the Monte Carlo simulations. The estimated number of collisions is also close to that observed in the simulations. This simple model thus provides a quick method of esti-

mating the survival distance of a neutron in any compound material, as a useful alternative to the more lengthy Monte Carlo simulations. It also confirms that the range in the detector material CH_2 (with or without Gd or Li loading) is much shorter than the range in the target material, as appropriate for capturing the neutrons preferentially in the detector. H_2O is also in this category, showing its unsuitability as a target material. Table 2 also includes the effect of variations in the scintillator loading, showing that beyond a certain level ($\approx 0.2\%$ in the case of ^6Li) further increase gives no significant change in neutron capture length (since the thermalisation distance is unchanged and becomes dominant). This is also confirmed by Monte Carlo simulation.

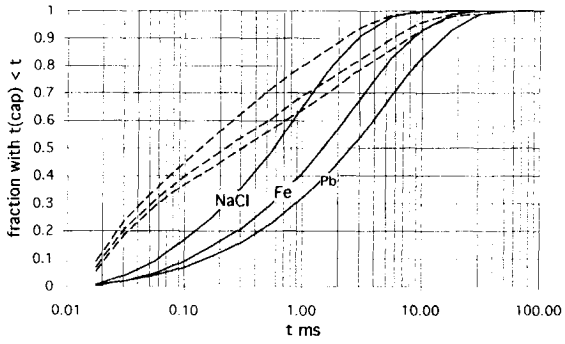

Fig. 9. Integral distributions of total neutron transit times (from rock to absorption in detector) for three target materials. *Full lines* show distributions for detector sheet thickness 2 cm. *Dashed lines* show corresponding distributions for detector sheet thickness 10 cm.

6. Variations in capture times

The multiple traversals of the cavern by the majority of the neutrons does not affect the discussion in Section 5 since the neutrons do not change energy or direction when crossing the cavern. However the total time between production and observation is substantially increased by this, so that it is important to check that variations in this detection time do not destroy the accuracy of the neutrino arrival time profile. Fig. 3 suggests that for neutrino mass estimates it will be sufficient to know the time profile with $\sim 5\%$ resolution. In addition, the statistics of 1000 events make it unlikely that the time binning could be shorter than 25 ms for the first 0.5 s, then 50–100 ms up to 4 s.

In the Monte Carlo simulations the total neutron travel time was summed for each event and a distribution of times was accumulated for those events captured in the detector. There are some geometry-dependent features found in the time distributions resulting from the fact that some neutrons are captured on first crossing the cavern, while others are captured on subsequent crossings. Smoothed integral distributions of the capture times are shown in Fig. 9, for two detector slab thicknesses (2 cm and 10 cm) and for three wall materials (NaCl, Fe, Pb). The longer times with the iron and lead walls are consistent with the discussion in Section 5, that the increased survival time in the iron would result in greater detection efficiency through more traversals of the cavern and hence longer times before capture by the detector. The longer times for the thinner (optimum) detector result from the passage of a neutron more than once through the detecting slab while being thermalised.

For salt caverns, 95% of the neutrons are detected within 4 ms (i.e., 2 ± 2 ms variation) and 80% within 1 ± 1 ms. For iron or lead-lined walls, $\sim 90\%$ of neutrons are detected within ~ 10–15 ms. These times are for typical individual salt mine caverns 10 m $\times$ 8 m $\times$ 6 m and would increase or decrease approximately in proportion to the linear size. For multi-target OMNIS schemes, shorter capture times could be achieved by alternating layers of scintillator and iron or lead targets.

7. Neutron background

Underground neutron background arises mainly from Th and U contamination of the rock, emitting alpha particles which interact with the rock elements to give an MeV-range spectrum similar to that produced by the neutrino interactions. There is also a contribution from U fission, but this is a factor 10 lower. For typical U and Th levels in salt mines (at the 10–100 ppm level) the neutron production is estimated to be within a factor 2 of 10^{-8} n g^{-1} s^{-1} consistent with measured neutron backgrounds [30]. This is continuous and can be subtracted, leaving the Poisson fluctuations in any time interval.

Since the supernova pulse and continuous background neutrons are both spatially uniform in the rock, with similar energy spectra, all signal/noise considerations are independent of detector geometry or efficiency, since this is the same for each. A neutrino burst at 8 kpc produces $\approx 1 \cdot 10^{-7}$ neutrons g^{-1} in the rock superimposed on the continuous production $\approx 1 \cdot 10^{-8}$ neutrons g^{-1} s^{-1}. Thus regardless of the detection efficiency if a total of N events is seen the continuous background will be 0.1 N events s^{-1}. If binned into intervals δt seconds there will be an average of 0.1 N δt background events in each bin. This number can be subtracted from each bin to leave Poisson fluctuations $\sim \sqrt{0.1 N \delta t}$. As an example, for a supernova signal of 1000 neutron events produced over a few seconds and binned into 0.1 s intervals, the cavern background fluctuations would be $\pm \sim 3$ counts in each 0.1 s interval, which for the first 2 s will be less than the Poisson fluctuations in the signal profile itself. An illustrative simulation of this, for 50 eV tau neutrino mass and < 5 eV mu neutrino mass, is shown in Fig. 10.

Alternative sites, e.g., those based on chalk or sandstone (silica) are in general found to have slightly higher levels of U and Th and hence proportionately higher continuous neutron background, but by a factor typically < 4. The background fluctuations are higher by only the square root of this, i.e., a factor ≤ 2 and this will in some cases be offset by the higher capture efficiency of these materials (Fig. 7). Thus the majority of underground sites would be suitable, apart from those in granite, which may have up to a factor 100 higher level of U and Th.

Another potential source of neutron background is the cosmic ray muon flux, which produce neutrons by nuclear spallation or capture. This background has been previously studied in some detail for underground dark matter experiments and estimates have been made of total neutron production rate and energy spectrum as a function of depth, taking into account the energy-dependent multiplicity [30]. Those arising from muon capture have energies 1–10 MeV, similar to those neutrino excitation. Those from spallation extend in energy up to $\sim$ 1000 MeV, but the higher energy does not significantly affect the thermalisation and capture length because of the logarithmic dependence of N_s on E_0 in Eq. (6b). Thus the background is again given simply by the total neutron production rate per gram of material, plotted as a function of depth in Fig. 11 (muon capture contribution estimated for medium-A materials). This shows that for any depth greater than 1500 mwe (i.e, $\sim$ 500 m), the rate for muon-produced neutrons is at least an order of magnitude lower than the rate $\sim 10^{-8}$ g^{-1} s^{-1} from U/Th alphas. This applies to the majority of established underground physics laboratories. For sites at or near the earth's surface the

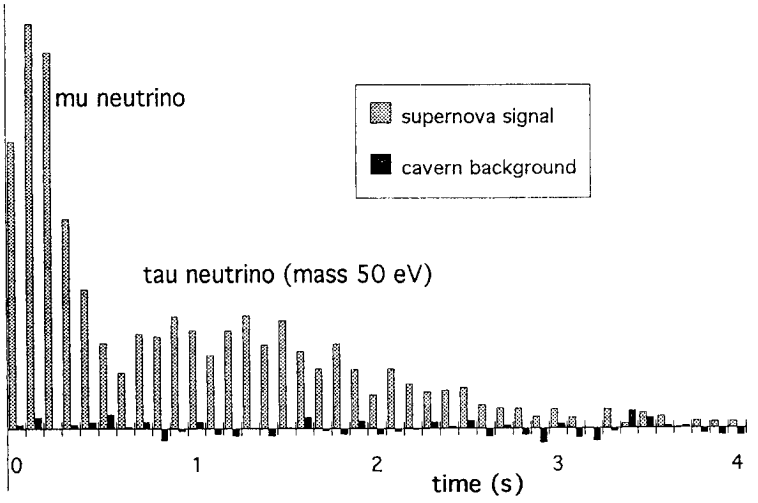

Fig. 10. Simulation of 1000-event arrival time profile of mu/tau neutrinos from 8 kpc Galactic supernova, binned in 0.1 s intervals with cavern background fluctuations shown separately for comparison. The profile corresponds to that of Fig. 3 for 50 eV tau neutrino mass.

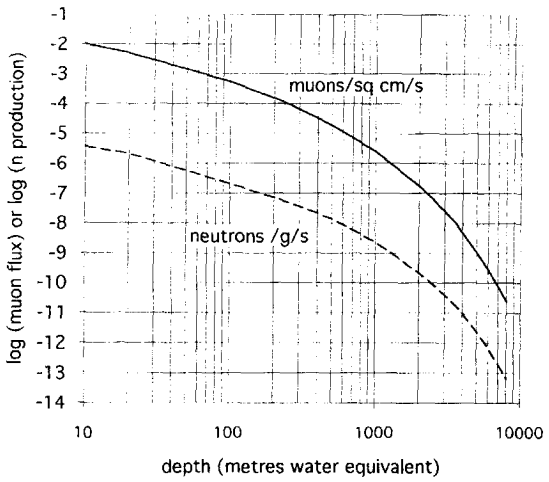

Fig. 11. *Full line*: cosmic ray muon flux vs. depth. *Dashed line*: estimated total neutron production rate vs. depth from muon spallation and capture.

muon interactions would dominate, giving a neutron production rate 10^{-6}–10^{-5} g^{-1} s^{-1} and background fluctuations an order of magnitude larger than those of Fig. 10, which would seriously distort the supernova profile. Thus underground operation of OMNIS appears essential, even with low background target materials.

The supernova signal falls below the cavern neutron background for times > 4 s. It would be of interest to be able to follow the time profile for longer times and this would be possible in principle by using refined Fe or Pb as the principal target material. Measured U and Th concentrations in these materials are typical a factor 10^4 lower than in natural rocks, reducing the alpha-n reactions to below the muon-produced rates in Fig. 11, which then become the main source of background. At a depth of 3000–3600 mwe, the continuous muon background neutron production would be $\sim 10^{-11}$ g^{-1} s^{-1}, reducing the square root background fluctuations by a factor 30 from those in Fig. 10 and allowing the time profile to be observed out to 20–50 s.

An alternative target material with very low intrinsic background would be frozen CO_2. Table 2 shows that this has a neutron survival distance (in g cm^{-2}) comparable to that of Fe and hence a similarly high value of detected neutrons/m^3 scintillator. This target material would be essentially free from U/Th contamination if, for example, extracted from the atmosphere by refrigeration of dry filtered air. The background would then be again reduced to the depth-dependent baseline from cosmic ray muons (Fig. 11).

8. Comparison of world supernova detectors

Table 1 compares the neutrino sensitivity of an illustrative example of OMNIS with that of direct detection in Super-Kamiokande, LVD, Macro and SNO (the latter with H_2O or D_2O targets). The figures for the direct detectors are taken from Ref. [3] in which the contributions from various interactions in these detectors are discussed in more detail. Event numbers are shown separately for ν_e, $\bar{\nu}_e$ and $\nu_{\mu,\tau} + \bar{\nu}_{\mu,\tau}$, for a supernova at 8 kpc. Direct detection in water or scintillator is sensitive principally to the ν_e component and none of these large detectors has the required ~ 2000 event $\nu_{\mu,\tau}$ detection capability except (marginally only) the D_2O target of SNO which may have a limited operational lifetime.

In contrast, the nuclear excitation principle has the unique property of observing a large $\nu_{\mu,\tau}$ signal with a relatively small contamination of ν_e, $\bar{\nu}_e$ events. The effective neutrino detection capability for a Pb/Fe/rock target array is 10 events/ton scintillator, a factor 30 greater than the 0.35 events/ton in MACRO and would provide 2000 mu/tau neutrino events for a scintillator mass of only ~ 200 tons (distributed along 200–400 m of tunnel or caverns). In effect, neutron collection provides a remarkable magnification factor – each 1 ton of scintillator registers the neutrino events from 50 tons of target. At the same time, the comparatively low detector mass ensures that there will be a correspondingly small number of direct (charged current) $\bar{\nu}_e$ events in the scintillator itself.

9. Requirements for extra-galactic supernova detection

Observations suggest [10,11] that supernova rates reach ~ 1 yr^{-1} at a distance ~ 4 Mpc and this has led to discussions of the feasibility of detection

systems large enough to observe the neutrino profile from that distance. The time-integrated neutrino flux is reduced from $\sim 10^{12}/\mathrm{cm}^2$ at 8 kpc to $4 \cdot 10^6/\mathrm{cm}^2$ at 4 Mpc, requiring a factor 500^2 scale up in target mass. This probably excludes from consideration any targets other than naturally-occurring (zero-cost) materials such as water or rock. SNBO/OMNIS is thus a natural candidate detection scheme, but would require instrumentation of the equivalent of $\sim 1\ \mathrm{km}^3$ underground rock. Although this would be precluded by the present economics of manufactured detectors, it can be envisaged that, perhaps within < 50 yr, current developments in nanochemistry and molecular self-assembly will lead to self-assembling materials and structures which render obsolete present manufacturing concepts [30]. This could enable large scale detector 'membranes' to be 'grown' over a period of time at essentially zero cost (analogous to biological growth). This would be particularly suited to the SNBO/OMNIS schemes, which can be adapted to any shape of target or neutron detector.

Accepting this as a conceptual possibility, there would still remain a serious neutron background problem. Since the supernova burst consists of a single pulse, the required detailed shape of its time profile cannot be extracted from random noise of larger amplitude, even if the start time is known from, for example, the signal from a gravitational wave detector [12,13]. Thus on the assumption that a 1000-event signal is required with a background level no more than a factor 2 higher than that achievable in the Galactic case (Fig. 3) it would be necessary to reduce the continuous neutron production by a factor $> 10^5$ and hence the U and Th levels in the target should be not higher than $\sim 10^{-13}$–10^{-14} (g/g). This is certainly possible in refined materials but not in natural rocks or natural water.

A candidate material available naturally in very large quantities, yet satisfying the low U/Th requirement, would be CO_2 (forming 0.3% of the atmosphere) which in solid form has already been noted in Section 7 to be potentially an excellent low-background target. In principle, over a period of 10–30 yr, this could be progressively condensed from the atmosphere to create large 'icebergs' which, for ~ 100 m radius, would have natural thermal survival times (i.e., without continuous refrigeration) of hundreds of years. As discussed in Section 7, the neutron production from muons must also be reduced to a level similar to that of the U/Th neutron production and this imposes a minimum depth for the detector. Table 3 compares the basic parameters for Galactic and extra-Galactic supernova detectors. Relaxing the constraints on time binning and background by a factor 2 for the extra-Galactic case, the muon flux limit becomes $< 2 \cdot 10^{-10}\ \mathrm{cm}^{-2}\ \mathrm{s}^{-1}$ which, using Fig. 11, translates to a minimum depth of 6000 mwe. Thus the background constraints could in principle be satisfied by sinking the CO_2 icebergs (density ~ 1.5) to the ocean floor, using the outer 2–3 m layer of solid CO_2 to provide passive shielding against neutron background from U and Th in the sea.

The construction of astrophysical detectors on the 1 km^3 scale is currently under discussion for gamma

Table 3
Comparison of basic parameters and background restrictions for Galactic and Extra-Galactic supernova detectors

	Unit	Galactic	Extra-Galactic
Target material		NaCl rock	Solid CO_2
Supernova distance	kpc	8	4000
Detected signal	events	1000	1000
Neutron burst in target	g^{-1}	$1 \cdot 10^{-7}$	$4 \cdot 10^{-13}$
Effective target mass	ton	10^4	$2.5 \cdot 10^9$
Time binning range	ms	10–100	20–200
Continuous n background limit	totals s^{-1}	< 500	< 1000
Background n from U and Th	$\mathrm{g}^{-1}\ \mathrm{s}^{-1}$	$< 2 \cdot 10^{-8}$	$< 1 \cdot 10^{-13}$
Required n limit from muons	$\mathrm{g}^{-1}\ \mathrm{s}^{-1}$	$< 2 \cdot 10^{-8}$	$< 4 \cdot 10^{-13}$
Muon flux limit	$\mathrm{cm}^{-2}\ \mathrm{s}^{-1}$	$< 2 \cdot 10^{-5}$	$< 2 \cdot 10^{-10}$
Minimum detector depth	mwe	500	6000

ray and high energy neutrino astronomy, using natural water or ice as the detecting medium [24,25], but these would not require detectors distributed so finely throughout the volume as in this case. Thus although it is possible in principle to visualise a configuration which would satisfy the ultra-low background requirements for an extra-Galactic supernova neutrino detector, no solution is yet in sight to the problem of low cost neutron detection and readout for such a large scale target. It is thus not clear whether such an extra-Galactic detector could ever be feasible, even assuming automated growth of the target itself.

10. Conclusions

A detailed study has been made of alternative forms of the Supernova Neutrino Burst Observatory proposed in 1990 by Cline et al., based on the detection of neutrons from neutral current excitation of nuclei in underground rock. Three stages of evolution of this have been studied:

- Stage I: Boron trifluoride neutron counters with polythene or wax thermalisation, embedded in the rock as originally proposed.
- Stage II: Improvements in neutron capture efficiency by location in open caverns, use of scintillator for combined thermalisation/absorption and optimisation of surface area/volume.
- Stage III: Use of supplementary target materials with improved neutron survival to further increase the number captured in the detector.

The combination of improvements in Stage II increases the event capture by a factor 20 compared with Stage I. The optimum detector geometry consists of large area slabs ~ 5–10 cm thick and loaded with 0.1%–1% ^{6}Li, ^{10}B or Gd for unambiguous signal identification. For a detector array giving 2000 $\nu_{\mu,\tau}$ events at 8 kpc, ~ 200 tons of scintillator would be required, each ton of detector effectively monitoring 50 tons rock. This is a factor 30 better than direct detection (of $\bar{\nu}_e$) in liquid scintillator.

Thus, in addition to its unique capability of observing a large tau/mu neutrino signal, this scheme offers the least expensive form of supernova detector. Preliminary cost estimates based on 0.5 ton modules indicate a total cost of detector and electronics in the region £50k/ton, or $\sim$£$5 \cdot 10^6$ per 1000 $\nu_{\mu,\tau}$ events from a supernova at 8 kpc. It is assumed that existing underground sites would be used. For the multi-target version, the cost of the additional target materials is approximately offset by the increased production in these, so that the unit cost (per event) is similar.

Neutron background from cosmic ray muons requires operation at a depth > 1500 mwe. In typical underground sites, neutron background fluctuations from U/Th radioactivity are found to be smaller than the Poisson fluctuations in the signal itself, for a Galactic supernova at distances up to about 20 kpc and thus comfortably allow the shape of the neutrino profile to be observed with sufficient accuracy to measure a neutrino mass in the 5–50 eV range. For the ~ 85–90% of Galactic supernovae not visible optically their distance R can be estimated initially from the electron antineutrino signal strength in several world detectors, subject to a factor ~ 2 uncertainty in the initial source strength S. Note that a neutrino mass estimate m_ν depends, from (1), on $R^{0.5}$ with the estimate of R dependent in turn on $S^{0.5}$. Thus the estimate of m_ν depends on $S^{0.25}$ and a factor 2 (1.5 ± 0.5) uncertainty in S reduces to an uncertainty of only $\pm 10\%$ in m_ν. More accurate confirmation of the distance would follow if the supernova can be subsequently located in infra-red and radio searches, assisted by the directional information from time delays between several separated neutrino detectors.

Scale up to extragalactic (4 Mpc) supernova detection would allow neutrino masses a factor 20 smaller to be measured and increase the supernova rate to 1 yr^{-1}. No natural underground locations would be suitable, but the factor 500^2 weaker signal could in principle be seen above background with an ultra-high purity target of solid carbon dioxide at an undersea depth of 6000 m. The total target size would be equivalent to ~ 1 km^3, instrumented with a prohibitive $\sim 5 \cdot 10^6$ m^3 of neutron detector. As discussed in Section 9, this would await a future era in which automated growth and self-assembly supersedes traditional manufacture.

In contrast, the Galactic observatory can be easily and inexpensively constructed with established neutron detection technology and materials. Since the neutron detector modules are linked to the rock target only by freely scattering neutrons, they can be

installed in any convenient position in existing operational underground sites and distributed between several caverns or tunnels. There is also no fixed size for the array – it is possible to begin by operating a smaller number of modules and increasing the array over a period of time. These modules should preferentially be distributed between 2–3 well-separated underground sites. Coincidences between sites would eliminate spurious muon-initiated multi-neutron showers [26] and allow also the possibility of discovering new astrophysical neutrino phenomena. This would also provide an estimate of the supernova direction through the arrival time differences.

We conclude that the relatively low cost of the OMNIS scheme makes it possible to propose a dedicated Galactic supernova neutrino observatory, capable of observing the time profile of the mu and tau neutrino component. This would provide the first direct measurement of a cosmologically-significant neutrino mass and the use of several different target elements, in conjunction with the large electron antineutrino signal from SuperKamiokande would also provide data on the presence or absence of neutrino mixing on the Galactic distance scale.

Acknowledgements

I acknowledge discussions over many years with D.B. Cline and G.M. Fuller on the original SNBO concepts; with J.R. Wilson, B. Cox, G. McLaughlin, C.K. Hargrove, on neutron production; with R.N. Boyd, D.A. Sanders, F. Boehm, J. Kleinfeller, R. Marshall, W. Vernon, R. Shirato, on detector design options; and with A. Burrows, E.E. Becklin, C.R. Kitchin on aspects of supernovae. Some of the work on underground neutron background rates and required event numbers was carried out in collaboration with J.D. Lewin.

References

[1] S.E. Woosley, T.A. Weaver, Ann. Rev. Astron. Astrophys. 24 (1986) 205.
[2] A. Burrows, Ann. Rev. Nucl. Part. Sci. 40 (1990) 181.
[3] A. Burrows, Phys. Rev. D45 (1992) 3361.
[4] R. Mayle, J.R. Wilson, D. Schramm, Ap. J. 318 (1987) 288.
[5] E.S. Myra, A. Burrows, Ap. J. 364 (1990) 222.
[6] D. Kielczewska, Int. J. Mod. Phys. D3 (1994) 331.
[7] Chengrui Ching, Tsohsiu Ho, Phys. Rep. 112 (1984) 1.
[8] P.F. Smith, J.D. Lewin, Phys. Lett. 127B (1983) 185.
[9] P.F. Smith, J.D. Lewin, Acta Physica Polonica B16 (1985) 837.
[10] S. Van der Bergh, G.A. Tammann, Ann. Rev. Astron. Astrophys. 29 (1991) 363.
[11] E.E. Becklin, Trends in Astroparticle Physics, Santa Monica, 1990, p. 496.
[12] D.B. Cline et al., Nucl. Phys. B 14A (1990) 348.
[13] D.B. Cline et al., Astro. Lett. Comm. 27 (1990) 403.
[14] D.B. Cline et al., Phys. Rev. D50 (1994) 720.
[15] S.E. Woosley et al., Ap. J. 356 (1990) 272.
[16] G.M. Fuller, B.S. Meyer, Ap. J. 376 (1991) 701.
[17] G.M. Fuller, B.S. Meyer, Ap. J. 453 (1995) 792.
[18] R. Marshall, Proc. Conf. Identification of Dark Matter, Sheffield, UK, 1996 (World Scientific, to be published).
[19] F. Boehm et al., Proc. TAUP95' Toledo, Nucl. Instrum. Meth. A300, 1991, p. 395, Elsevier (to be published).
[20] M. Abbes et al., Nucl. Instrum. Meth. A374 (1996) 164.
[21] G.F. Knoll, Radiation Detection and Measurement, Wiley, 1979.
[22] C.K. Hargrove et al., Astropart. Phys. 5 (1996) 183.
[23] G. McLaughlin, G.M. Fuller, in preparation.
[24] F. Halzen, G. Jakzko, Phys. Rev. D54 (1996) 2779.
[25] J. G. Learned, Proc. Texas/ESO-CERN Symposium, Ann. N.Y. Acad. Sci., Vol. 647 (1991) p. 464.
[26] B. Stella et al., Nucl. Instrum. Meth. A355 (1995) 609.
[27] B. Cox, Manchester, personal communication, 1995.
[28] G.M. Fuller, personal communication.
[29] Scintillator Product Brochure, BICRON, Newbury, OH.
[30] J.D. Lewin, personal communication.